Adsorption (2007) 13: 373–383
DOI 10.1007/s10450-007-9020-x

Separation of carbon dioxide/methane mixtures by adsorption on a basic resin

José A. Delgado, · María A. Uguina · José L. Sotelo · Beatriz Ruíz · Marcio Rosário

Received: 14 February 2007 / Revised: 9 July 2007 / Accepted: 11 July 2007 / Published online: 20 September 2007

Abstract In this work, the separation of carbon dioxide/methane mixtures by PSA using a basic resin (Amberlite IRA-900) has been studied. Adsorption equilibrium and kinetics of carbon dioxide and methane on a fixed-bed of this adsorbent have been measured, and a binary adsorption equilibrium isotherm has been obtained. The adsorbent deactivation with the number of adsorption-desorption cycles, and its regeneration, have also been analysed. A model based on the LDF approximation has been used to describe the experimental breakthrough curves. The applicability of the basic resin to the separation of carbon dioxide/methane mixtures has been studied in an experimental PSA setup using a single bed. The validity of the model used in the fixed-bed study for simulating a PSA system has been checked by comparing the simulated and the experimental performance of the proposed PSA cycle.

Keywords Carbon dioxide · Methane · Basic resin · Amberlite IRA-900 · Adsorption · Fixed-bed · PSA

Abbreviations

A	parameter defined in (4)
b	adsorption affinity, Pa^{-1}
B	parameter defined in (4), K
b_0	parameter defined in (4)
c	concentration, $mol\,m^{-3}$
D	diffusivity, $m^2\,s^{-1}$
D_L	axial dispersion coefficient, $m^2\,s^{-1}$
E	parameter defined in (4)
E_0	stagnant contribution to axial dispersion
f	empirical interaction parameter
ΔH	adsorption enthalpy, $J\,mol^{-1}$
k_f	external mass transfer coefficient, $m\,s^{-1}$
K_H	Henry's law constant, $mol\,kg^{-1}\,Pa^{-1}$
k_s	lumped mass transfer coefficient, s^{-1}
N	adsorption rate, $mol\,m^{-3}\,s^{-1}$
n	parameter defined in (4)
P	total pressure, Pa
p	partial pressure, Pa
Q	volumetric flow rate, $m^3\,s^{-1}$
q	adsorbed concentration, $mol\,kg^{-1}$
q^*	adsorbed concentration in equilibrium with the gas phase, $mol\,kg^{-1}$
$\overline{q}$	average adsorbed concentration, $mol\,kg^{-1}$
q_{max}	maximum adsorption capacity, $mol\,kg^{-1}$
R	gas constant, $8.31\,J\,mol^{-1}\,K^{-1}$
Re	particle Reynolds number, $u\rho_g 2r_p/\mu$
r_p	particle radius, m
Sc	Schmidt number, $\mu/(\rho_g D_m)$
t	time, s
T	temperature, K
u	superficial velocity, $m\,s^{-1}$
y	mole fraction in the gas phase

Greek symbols

ε	bed voidage fraction
ε_p	particle porosity
μ	gas viscosity, Pa s
ρ	density, $kg\,m^{-3}$
τ	tortuosity

Subscripts and superscripts

0	initial

J.A. Delgado, (✉) · M.A. Uguina · J.L. Sotelo · B. Ruíz · M. Rosário
Department of Chemical Engineering, Universidad Complutense de Madrid, 28040, Madrid, Spain
e-mail: jadeldob@quim.ucm.es

F feed
g gas
H high pressure
i ith component
L low pressure
m molecular

1 Introduction

Methane is the most important non-CO_2 greenhouse gas responsible for global warming, and its warming effect is even higher than the one of carbon dioxide. Landfill gas (LFG) constitutes one of the main sources of methane emissions in many countries. This gas is released from aerobic decomposition of organic residues in municipal solid wastes. It is a multicomponent mixture containing mainly methane and carbon dioxide while many other gases are present at concentrations typically below 1%. The molar fraction of methane in LFG is between 0.45 and 0.65, balanced by carbon dioxide and contaminants (Cavenati et al. 2005). Therefore, LFG can be considered as a source of natural gas. This reason, together with the need of controlling the methane emissions to meet Kyoto Protocol targets, makes it very interesting to use this gas for energy production. For this purpose, it is necessary to reduce the carbon dioxide content of LFG. Moreover, carbon dioxide is not simply an inert, but also can be corrosive. It must be removed from natural gas prior to low temperature processing for NGL recovery. Generally, pipeline specifications for natural gas require a carbon dioxide concentration below 2–3% (Li et al. 2005).

The technology most widely used for carbon dioxide removal is amine absorption, but amine plants are complex and costly. Another alternative is to reduce the carbon dioxide content using an adsorption process. Pressure swing adsorption (PSA) technology has gained interest due to low energy requirements and low capital investment costs. For example, in the capture of carbon dioxide from flue gases, the energetic cost per ton of recovered carbon dioxide is about is about 335 kWh for an amine absorption process, whereas this value is about 170 kWh for a PSA process (Khoo and Tan 2006). The main requirement for this technology to be viable is to find an adequate adsorbent, which must be selective to one of the components of the carbon dioxide/methane mixture, but the affinity to the selected component cannot be too high, because in this case the regeneration of the adsorbent is compromised. Also, the uptake rates must be high in order to work with short cycles and high productivity.

Because of the interest of the carbon dioxide/methane separation, new technologies are under research, as well as new adsorbents, to make possible a better separation. Separation by PSA can be based either on the different adsorption affinity of the components (equilibrium separation), or on the different diffusion rates in the adsorbent (kinetic separation) (Ruthven et al. 1994; Yang 1997). A process for the recovery of methane from landfill gases was developed using a narrow-pore carbon molecular sieve (Schroter and Juntgen 1989; Pilarczyk and Knoblauch 1988). Carbon dioxide diffuses into the adsorbent much faster than methane, which is obtained as the raffinate product in the effluent stream, with a product purity of 87–89%. Kapoor and Yang (1989) have also studied the kinetic separation of a carbon dioxide/methane mixture (50/50) using a carbon molecular sieve, obtaining 90% methane with a productivity of 0.05 kg methane kg adsorbent^{-1} h^{-1}. Gomes and Hassan (2001) have investigated the feasibility of coalseam methane recovery with a VSA process using a carbon molecular sieve as the sorbent, obtaining a 90% methane product from a 50/50 carbon dioxide/methane mixture. Other process using an adsorbent kinetically selective to carbon dioxide for carbon dioxide removal from natural gas (ETS-4 zeolite) is currently offered by Engelhard Corporation. This process is able to treat economically a natural gas containing 38% of carbon dioxide and reduce this concentration below 2% (Engelhard Corporation 2005). Recently, the upgrade of methane from a carbon dioxide/methane mixture by pressure swing adsorption using a Takeda Carbon Molecular Sieve 3K has been studied experimentally by Cavenati et al. (2005). Purity higher than 96% can be obtained from a 45/55 carbon dioxide/methane mixture.

In this work, the separation of carbon dioxide/methane mixtures by PSA using a basic resin (Amberlite IRA-900) has been studied. This adsorbent has been selected because it has been reported that basic ion exchange resins are excellent sorbents for carbon dioxide (Yang 2003). Moreover, the selected resin is a macroreticular one, having an open structure which facilitates the mass transfer between the gas and the adsorbent surface. Adsorption equilibrium and kinetics of carbon dioxide and methane on a fixed-bed of this adsorbent have been measured, and a binary adsorption equilibrium isotherm has been obtained. The adsorbent deactivation with the number of adsorption-desorption cycles, and its regeneration, have also been analysed. A model based on the LDF approximation has been used to describe the experimental breakthrough curves. The applicability of the basic resin to the separation of carbon dioxide/methane mixtures has been studied in an experimental PSA setup using a single bed. The validity of the model used in the fixed-bed study for simulating a PSA system has been checked by comparing the simulated and the experimental performance of the proposed PSA cycle.

2 Experimental section

All the gases used in this work had purity higher than 99.5%, supplied by Praxair. The adsorbent used was Am-

Table 1 Properties of the adsorbent and the fixed-bed

Adsorbent	
Particle radius	0.28 mm (average)
Particle density	855 kg m^{-3}
Particle porosity	0.292
BET area	22 m^2 g^{-1}
Fixed-bed	
Bed length	0.125 m
Bed weight	12.6 g
Bed internal diameter	0.016 m
Bed voidage fraction	0.42

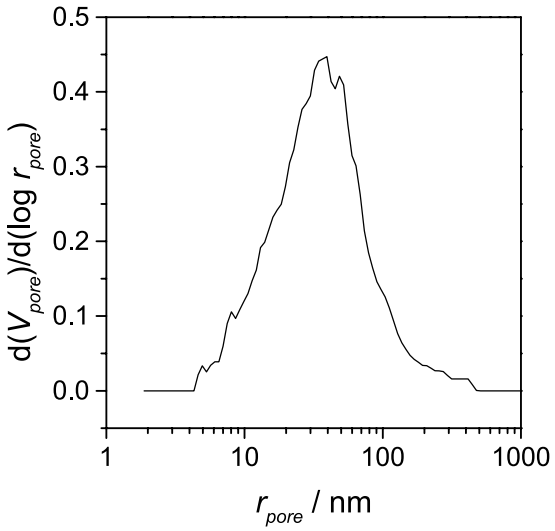

Fig. 1 Pore size distribution of Amberlite IRA-900 estimated by Hg porosimetry

berlite IRA-900 in chloride form, supplied by Fluka. Before use, it was washed with methanol in a Soxhlet extractor until the color of the methanol in contact with the resin disappeared. Afterwards, it was put in a column and contacted with a solution of NaOH 1 M until the pH at the exit and the inlet of the column was the same. Secondly, it was washed with ultrapure water until the pH at the column exit was neutral. Finally, it was dried overnight at 50 °C. The regeneration of the resin used in the adsorption experiments was performed subjecting it to the treatment with NaOH again. The adsorbent physical properties and its pore size distribution (estimated by nitrogen- and Hg-porosimetry) are shown in Table 1 and Fig. 1 respectively.

The fixed-bed experiments were carried out in an experimental setup described elsewhere (Delgado et al. 2006a). This setup was modified in order to perform PSA experiments, changing the configuration of the connections and introducing four solenoid valves (Electrotraz 012C-2) controlled by a computer (Fig. 2).

The low pressure in the PSA cycle was obtained with a membrane vacuum pump (Edwards Dlab 10-8), and this pressure was measured and controlled with vacuum controller connected to the pump (Buchi B-721). The solenoid valves could be opened or closed at specified times using a control program (Control-CB), installed in a computer equipped with an interface card (CIO-DIO24) connected to the valves. The volume of the gas produced in the PSA cycles was measured with a bubblemeter.

Equilibrium data at high pressures were obtained in a volumetric installation described elsewhere (Delgado et al. 2006b).

3 Model description

The model used to describe the fixed-bed and PSA dynamics is derived from the mass, energy and momentum balances, including the following assumptions:

(i) The flow pattern is described with the axially dispersed plug flow model
(ii) Local thermal equilibrium is assumed between the gas and the adsorbent particles
(iii) The mass transfer rate is represented by a linear driving force (LDF) model
(iv) The gas phase behaves as an ideal gas mixture
(v) Radial concentration and temperature gradients are negligible.

The partial differential equations and the corresponding boundary conditions of this model have been described in a previous work (Delgado et al. 2006a). The complete model was solved numerically using the PDECOL program (Madsen and Sincovec 1979), which uses orthogonal collocation on finite elements technique. The adsorption equilibrium isotherm employed is the extended Langmuir equation. This model was selected because it reproduces the experimental data adequately, and because it is introduced in the computer program for the numerical integration easily. A term taking into account the amount of gas retained in the adsorbent pores was added to this isotherm (Sircar and Kumar 1983):

$$q_i = \frac{P y_i \varepsilon_p}{RT\rho_p} + \frac{q_{\max,i} b_i P y_i}{1 + \sum_{j=1}^{j=n} b_j P y_j}. \quad (1)$$

This term may be significant for the gases that do not adsorb strongly, where ε_p represents the total internal porosity (m^3 void/m^3 particle). Considering the low BET surface area of the adsorbent (22 m^2 g^{-1}), and the pore size distribution estimated by Hg porosimetry (Fig. 1), it may be deduced that this porosity comes from meso- and macropores, whereas micropores are not detectable. Although this equation has no fundamental basis, it allows accounting for

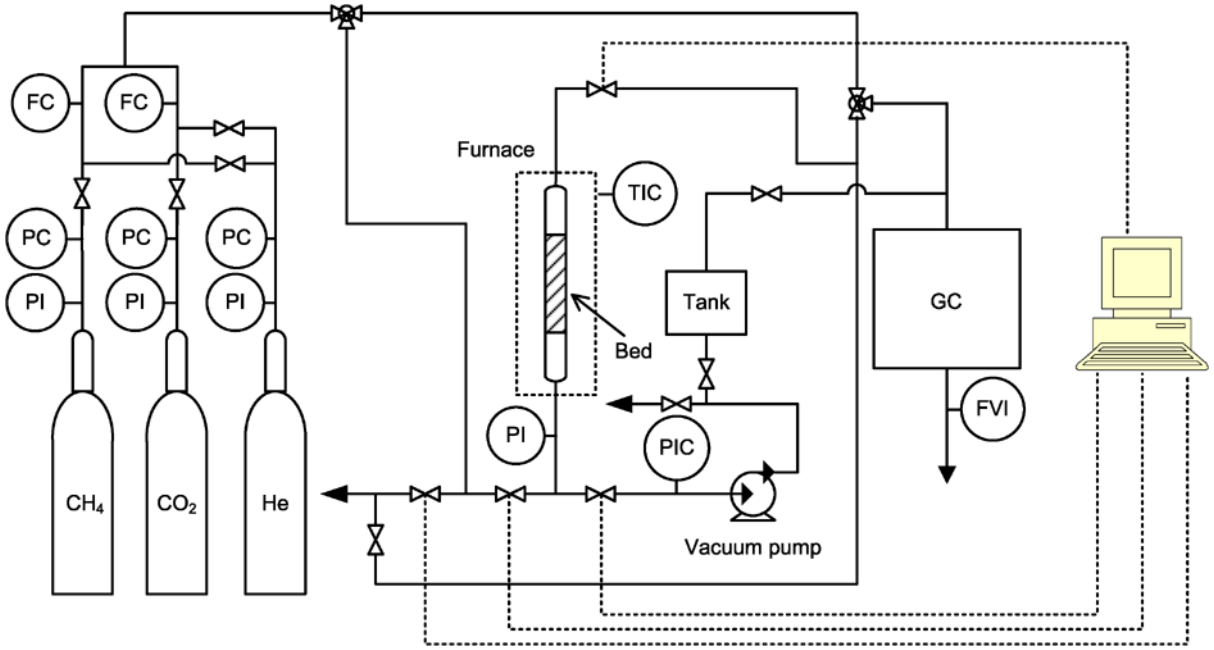

Fig. 2 Scheme of the setup for the PSA experiments

the gas retained inside the pores in the mass balance in the adsorbent particles when the LDF approximation is used (2):

$$N_i = (1-\varepsilon)\rho_p \frac{\partial \overline{q_i}}{\partial t} = (1-\varepsilon)\rho_p k_{s,i}(q_i^* - \overline{q_i}) \tag{2}$$

where N_i is the rate of adsorption of each component (in $\mathrm{mol_i\,m^{-3}_{bed}\,s^{-1}}$) and $k_{s,i}$ is a lumped mass transfer coefficient considering all the resistances present in the system. The breakthrough curves of carbon dioxide-helium and methane-helium mixtures predicted with using (1) and (2) in the complete model were compared with the ones obtained considering the accumulation of gas within the adsorbent pores with a more physically sound equation, assuming that the gas inside the pores is in equilibrium with the adsorbed phase in (2), and eliminating the first term in (1):

$$N_i = (1-\varepsilon)\left(\rho_p + \varepsilon_p \left.\frac{dc_i}{dq_i}\right|_{\overline{q_i}}\right)\frac{\partial \overline{q_i}}{\partial t} = (1-\varepsilon) \times \left(\rho_p + \varepsilon_p \left.\frac{dc_i}{dq_i}\right|_{\overline{q_i}}\right) k_{s,i}(q_i^* - \overline{q_i}) \tag{3}$$

where the term $dc_i/d\overline{q_i}$ is deduced from the isotherm equation. The breakthrough curves obtained with both approaches were practically identical. The first approach was used in this work because it has the advantage that the stiffness of the differential equations is lower, and the numerical integration is thus easier.

4 Results and discussion

4.1 Study of the decrease of the carbon dioxide adsorption capacity with the number of adsorption-desorption cycles

In preliminary experiments, it was observed that the carbon dioxide adsorption capacity of a bed of basic resin decreased slowly with the number of adsorption-desorption cycles. Each cycle was composed of an adsorption step, where the breakthrough curve of a carbon dioxide-helium mixture was obtained, and the corresponding adsorption capacity measured (as it is discussed in the following section), and a desorption step, where the bed was evacuated for 30 min, and purged with helium for 30 min. These decrease was estimated as the reduction of the Henry's law constant for this system, shown in Fig. 3, calculated as $q/(Py_F)$, where y_F is about 0.13. This concentration falls within the linear part of the adsorption isotherm.

After about 16 cycles, the adsorption capacity has decreased about a 28%, reaching a constant value. A quite similar behavior has been observed in the adsorption of carbon dioxide in hydrotalcite (Yong and Rodrigues 2002), which is also a basic adsorbent. This decrease of adsorption capacity could be ascribed to the irreversible adsorption of a certain portion of the carbon dioxide (Yong and Rodrigues 2002). This portion is probably chemisorbed in the form of carbonates, taking into account the basic character of the adsorbent. The PSA experiments and the ones used for determining the equilibrium parameters, discussed in the next sections, were

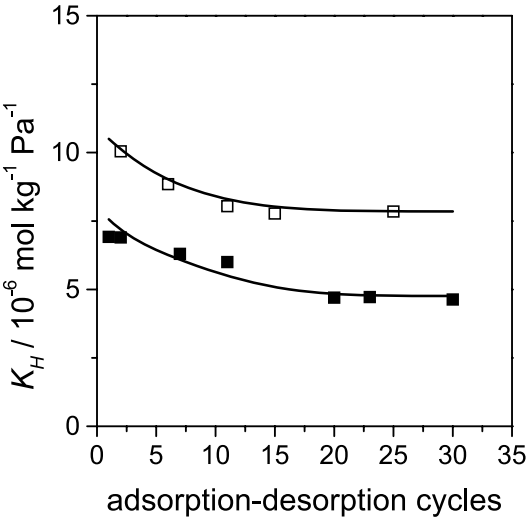

Fig. 3 Variation of the Henry's law constant (K_H) for the carbon dioxide-Amberlite IRA-900 system with the number of adsorption-desorption cycles. *Full squares*, adsorption data obtained five months after the preparation of the resin in OH-form. *Open squares*, data obtained just after treating the resin already used in the carbon dioxide adsorption fixed-bed experiments with NaOH

performed when the adsorption capacity of the bed was already stabilized.

In order to recover the initial adsorption capacity, and considering the hypothesis that the loss of capacity is due to the formation of carbonates on the surface, the used resin was treated again with NaOH (see Sect. 2), so as to eliminate the chemisorbed species. The adsorbent was then subjected again to several adsorption-desorption cycles, and the resulting dependence of the Henry's law constant with the number of cycles is shown in Fig. 3. It is observed that the adsorbent capacity is recovered, being even higher than the initial one of the adsorbent treated once with NaOH, and that it follows the same trend as before with the number of cycles. The higher capacity of the adsorbent treated twice with NaOH is attributed to the fact that it was used in the adsorption experiments just after the treatment with NaOH, whereas the first set of experiments were performed five months after the adsorbent was prepared, so that the resin could have suffered an aging process, probably a loss of moisture and some shrinking during this time. This aging was also observed in other process studied in our laboratories, the epoxidation of terpenes. When the resin was used as a catalyst in this reaction, the initial activity was higher than the one observed after several months.

4.2 Adsorption equilibrium of carbon dioxide and methane

The basic information required for designing an adsorption separation system are the equilibrium isotherms of the components to be separated. The adsorption equilibrium isotherms of carbon dioxide and methane were first obtained in the fixed-bed setup, estimating the adsorbed concentration as a function of the feed concentration from a mass balance in the fixed-bed. This method has been described in a previous work (Delgado et al. 2006a). The fixed-bed parameters are given in Table 1, and the experimental conditions and the resulting adsorbed concentrations are shown in Table 2.

The resulting isotherms at 298 K are shown in Fig. 4a. These data were fitted with the Langmuir model ($q = q_{max} bp/(1 + bp)$).

For methane, the experimental isotherm is linear, so only the Henry's law constant ($q_{max} b$) could be estimated. The Arrhenius plot of the Henry's law constant for both adsorbates is shown in Fig. 4b, and the estimated parameters are given in Table 3.

Both the Henry's law constants and the adsorption enthalpies of carbon dioxide and methane are significantly lower than the ones obtained in silicalite in a previous work ($2.16 \cdot 10^{-5}$ mol kg^{-1} Pa^{-1}, 24.6 kJ mol^{-1} for carbon dioxide, and $5.34 \cdot 10^{-6}$ mol kg^{-1} Pa^{-1} and 18 kJ mol^{-1} for methane) (Delgado et al. 2006a). The lower equilibrium constants in Amberlite IRA-900 can be attributed to the much lower BET surface area of this adsorbent (22 versus 337 m^2 g^{-1} for silicalite). The lower adsorption enthalpy for methane can be attributed to the much larger pore size of the basic resin. However, despite the effect of pore size, the lower adsorption enthalpy of carbon dioxide in Amberlite IRA-900 was surprising, because it was expected that the interaction of carbon dioxide with the basic groups of Amberlite IRA-900 was stronger than the one caused by dispersion forces in silicalite, taking into account the acid character of carbon dioxide. In order to verify the accuracy of the estimated adsorption enthalpy of carbon dioxide in this adsorbent, additional adsorption equilibrium data at different temperatures and higher pressures were obtained in a volumetric installation. The results are shown in Fig. 5.

The data represented with open symbols in this figure were calculated with the Langmuir parameters estimated previously, confirming the validity of the data obtained in the fixed-bed installation. The new data could be fitted very well with the Sips model, including temperature dependent parameters (Do 1998):

$$q = \frac{q_{\max}(bp)^n}{1 + (bp)^n} \quad b = b_0 \exp\left(\frac{E}{RT}\right) \quad n = A - \frac{B}{T} \tag{4}$$

where b_0, E, A and B were the fitted parameters. In this model, the parameter B was set equal to zero, so that the parameter E is directly the adsorption enthalpy, since this variable is no longer dependent on adsorbent loading in this case. The parameter q_{max} was set to the value corresponding to the total filling of pores with liquid carbon dioxide. The estimated values of the parameters are the following: $q_{max} = 9.92$ mol kg^{-1}, $b_0 = 8.277 \cdot 10^{-12}$ Pa^{-1}, $E = 19.4$ kJ mol^{-1}, $A = 0.57$ and $B = 0$. From this results, it is clear

Table 2 Experimental conditions for the runs carried out with carbon dioxide-helium and methane-helium mixtures

Run	Adsorbate	P_0 (Pa)	y_F	Q ($m^3\,s^{-1}$)	T (K)	q ($mol\,kg^{-1}$)
1	CO_2	$9.55\cdot10^4$	0.13	$4.03\cdot10^{-7}$	298	0.056
2	CO_2	$9.55\cdot10^4$	0.16	$4.19\cdot10^{-7}$	298	0.072
3	CO_2	$9.49\cdot10^4$	0.30	$4.26\cdot10^{-7}$	298	0.105
4	CO_2	$9.49\cdot10^4$	0.32	$3.41\cdot10^{-7}$	298	0.128
5	CO_2	$9.55\cdot10^4$	0.52	$2.82\cdot10^{-7}$	298	0.174
6	CO_2	$9.55\cdot10^4$	0.57	$2.79\cdot10^{-7}$	298	0.195
7	CO_2	$9.53\cdot10^4$	0.33	$1.85\cdot10^{-7}$	298	0.131
8	CO_2	$9.48\cdot10^4$	0.15	$4.20\cdot10^{-7}$	308	0.049
9	CO_2	$9.30\cdot10^4$	0.14	$4.25\cdot10^{-7}$	308	0.044
10	CO_2	$9.48\cdot10^4$	0.14	$4.39\cdot10^{-7}$	318	0.037
11	CH_4	$9.53\cdot10^4$	0.10	$2.93\cdot10^{-7}$	298	0.010
12	CH_4	$9.49\cdot10^4$	0.14	$1.85\cdot10^{-7}$	298	0.016
13	CH_4	$9.49\cdot10^4$	0.16	$2.49\cdot10^{-7}$	298	0.018
14	CH_4	$9.42\cdot10^4$	0.21	$1.43\cdot10^{-7}$	298	0.024
15	CH_4	$9.42\cdot10^4$	0.23	$1.40\cdot10^{-7}$	298	0.026
16	CH_4	$9.49\cdot10^4$	0.30	$2.28\cdot10^{-7}$	298	0.030
17	CH_4	$9.49\cdot10^4$	0.37	$1.79\cdot10^{-7}$	298	0.044
18	CH_4	$9.53\cdot10^4$	0.15	$2.49\cdot10^{-7}$	298	0.017
19	CH_4	$9.53\cdot10^4$	0.22	$1.48\cdot10^{-7}$	308	0.022
20	CH_4	$9.53\cdot10^4$	0.22	$1.56\cdot10^{-7}$	318	0.021

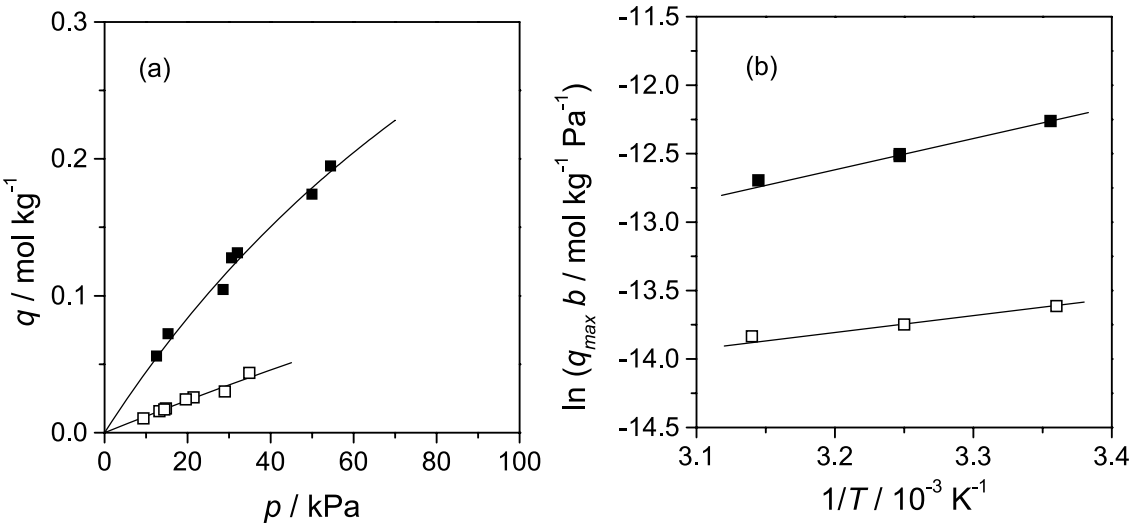

Fig. 4 Adsorption equilibrium data of carbon dioxide (*full squares*) and methane (*open squares*) on Amberlite IRA-900. (**a**) Experimental and fitted equilibrium isotherms at 298 K, (**b**) Arrhenius plot of the Henry's law constant ($q_{max}b$)

Table 3 Adsorption equilibrium parameters of the Langmuir model on Amberlite IRA-900

Gas	$q_{max}b_{298\,K}$ ($mol\,kg^{-1}\,Pa^{-1}$) ($mol\,kg^{-1}\,Pa^{-1}$)	q_{max} ($mol\,kg^{-1}$) ($mol\,kg^{-1}$)	ΔH ($kJ\,mol^{-1}$) ($kJ\,mol^{-1}$)
CO_2	$4.73\cdot10^{-6}$	0.73	19.0
CH_4	$1.22\cdot10^{-6}$	–	10.2

that the adsorption enthalpy of carbon dioxide estimated previously (19 $kJ\,mol^{-1}$) is realistic. This value is similar to the one estimated for the adsorption of carbon dioxide on several kinds of activated carbon, such as PCB (Calgon Corp.) and Nuxit-AL (Valenzuela and Myers 1989), which indicates that the interaction energy with the basic resin surface (once the stronger adsorption sites are occupied in several adsorption-desorption cycles, as discussed in the previ-

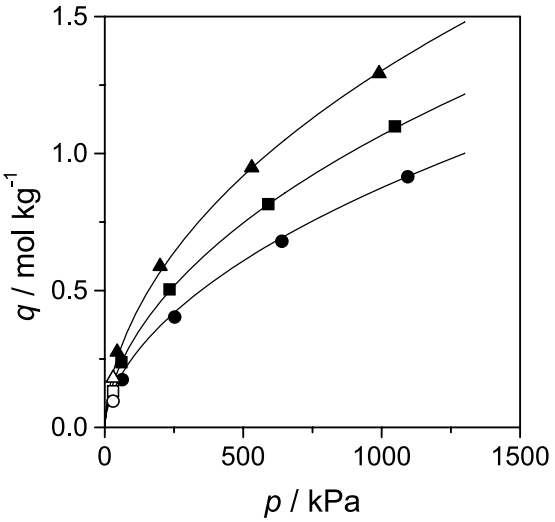

Fig. 5 Adsorption equilibrium data of carbon dioxide on Amberlite IRA-900 at high pressures obtained in a volumetric installation. *Full triangles*, 279 K. *Full squares*, 293 K. *Full circles*, 308 K. The *continuous lines* are the fitted isotherms with the Sips model. The *open symbols* were obtained with the Langmuir model, introducing the parameters estimated in the fixed-bed setup

ous section) is not enhanced by the acid character of carbon dioxide, being of physical nature.

4.3 Modeling of the breakthrough curves with carbon dioxide-helium and methane-helium mixtures

Adsorption kinetics is also an important aspect included in the basic information required for designing an adsorption system. If a fixed-bed configuration is employed, the proposed kinetic model must be able to predict the evolution of the concentration profiles inside the bed (and the temperature profiles if the temperature variations are important), and hence the breakthrough curves of the separated components. Firstly, the experimental breakthrough curves obtained with carbon dioxide-helium and methane-helium mixtures were analyzed, which are shown in Figs. 6 and 7. The model used for this purpose, outlined in Sect. 3, is described with more detail in a previous work (Delgado et al. 2006a), where the separation of the same gas mixtures using silicalite as the adsorbent were studied. This model was proposed following the work of Da Silva and Rodrigues (2001), introducing simplifications to reduce the computational time: a lumped mass transfer coefficient is used instead of considering two mass transfer resistances, and local thermal equilibrium is considered instead of taking into account the resistance to heat transfer between the adsorbent and the gas in the bed. This model was also able to reproduce the curves obtained with the Amberlite IRA-900 column, introducing the new experimental conditions (Tables 1 and 2), and changing the parameters of the Langmuir isotherm for each adsorbate (Table 3), the axial dispersion coefficient and the LDF kinetic

Table 4 Experimental conditions for the runs performed with carbon dioxide-methane mixtures

Run	P_0 (Pa)	y_{FCO2}	Q ($m^3\ s^{-1}$)	T (K)
21	$9.38{\cdot}10^4$	0.19	$2.20{\cdot}10^{-7}$	298
22	$9.38{\cdot}10^4$	0.27	$1.61{\cdot}10^{-7}$	298
23	$9.53{\cdot}10^4$	0.32	$1.23{\cdot}10^{-7}$	298
24	$9.41{\cdot}10^4$	0.48	$1.56{\cdot}10^{-7}$	298
25	$9.41{\cdot}10^4$	0.46	$1.60{\cdot}10^{-7}$	318
26	$9.45{\cdot}10^4$	0.56	$2.17{\cdot}10^{-7}$	298
27	$9.43{\cdot}10^4$	0.57	$1.80{\cdot}10^{-7}$	298
28	$9.42{\cdot}10^4$	0.57	$1.10{\cdot}10^{-7}$	298

parameters of each adsorbate. The axial dispersion coefficient was estimated with the correlation of Wakao et al. (1978).

$$D_{L,i} = \frac{D_{m,i}}{\varepsilon}(E_0 + 0.5ScRe) \tag{5}$$

where E_0 is the term corresponding to the stagnant contribution to axial dispersion. It was found that the value of this parameter for the Amberlite IRA-900 column was 0.13. This value is quite similar to the one estimated from data reported by Levenspiel (1999), 0.15, for the values of *Sc* and *Re* used in this work ($Sc \approx 1$, $Re \approx 0.01$–0.02).

The value of the LDF parameter of each component was estimated with the expression proposed by Farooq and Ruthven (1990), adapted to the macroporous resin used in this work:

$$k_{s,i} = \left[\frac{r_p q_{iF}}{3k_f P y_{iF}} + \frac{r_p^2 q_{iF}\tau}{15\varepsilon_p D_{i\text{-}He} P y_{iF}}\right]^{-1} \tag{6}$$

where r_p is the particle radius, k_f is the external mass transfer coefficient, τ is the tortuosity of the macropore network. The variables y_{iF} and q_{iF} are the molar fraction of component i in the feed and the corresponding equilibrium adsorbed concentration.

Figures 6 and 7 show a comparison among the theoretical and the experimental breakthrough curves for carbon dioxide and methane, respectively, where it can be observed that the model reproduces the experimental data satisfactorily for the different feed concentrations, flow rates and temperatures used.

4.4 Modeling of the breakthrough curves with carbon dioxide-methane mixtures

The validity of the model for predicting the breakthrough curves obtained with carbon dioxide-methane mixtures was studied. A set of breakthrough curves were obtained with this mixture, which are shown in Fig. 8. The experimental conditions are given in Table 4.

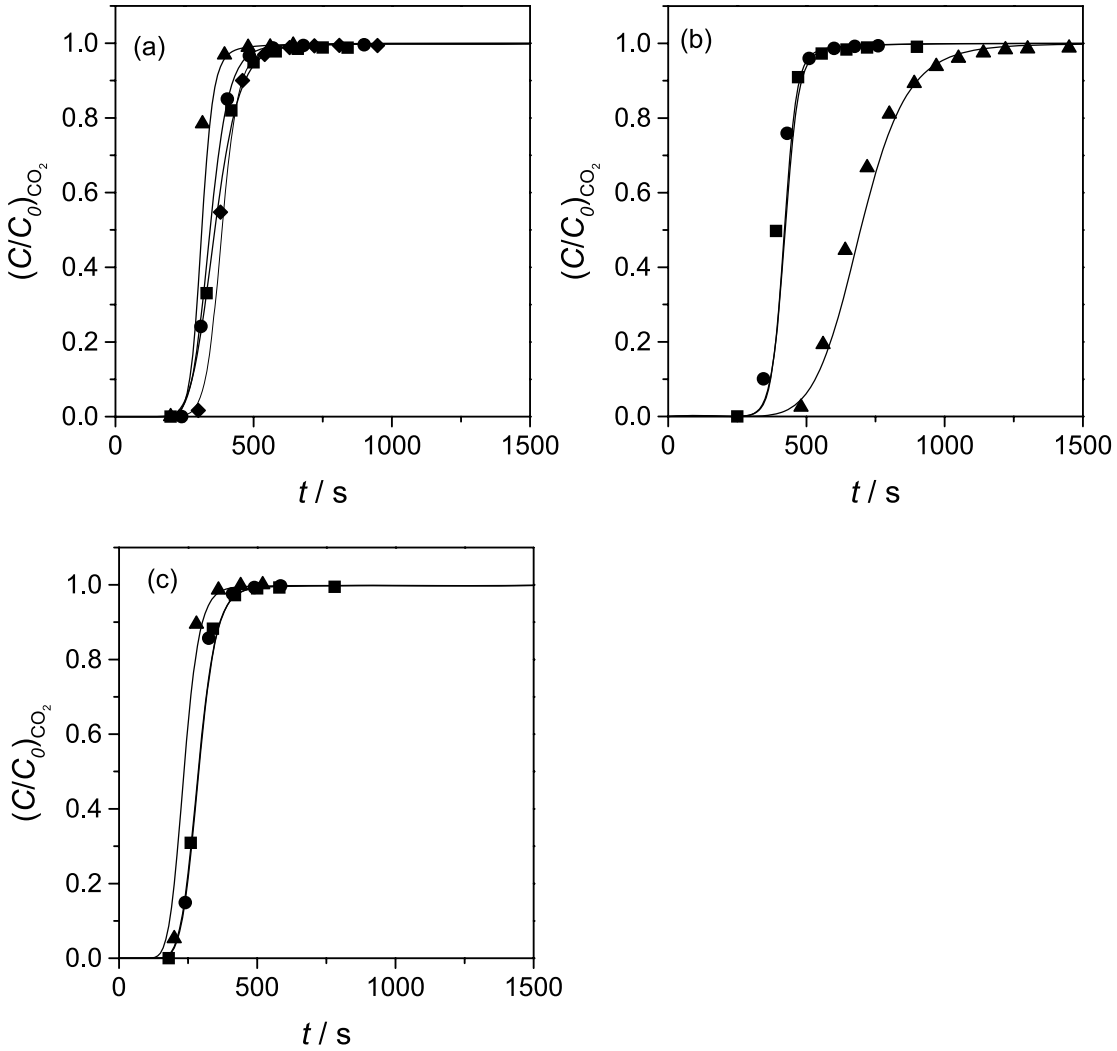

Fig. 6 Breakthrough curves of CO_2−He mixtures in Amberlite IRA-900. Experimental conditions in Table 2. *Continuous lines* are obtained with the model. (**a**) *Squares*, Run 1; *circles*, Run 2; *triangles*, Run 3; *diamonds*, Run 4. (**b**) *Squares*, Run 5; *circles*, Run 6; *triangles*, Run 7. (**c**) *Squares*, Run 8; *circles*, Run 9; *triangles*, Run 10

The experimental curves were compared with the theoretical ones obtained with the model, introducing the adsorption equilibrium parameters of carbon dioxide and methane in (1), and introducing the physical properties and transport parameters corresponding to carbon dioxide-methane mixtures (Delgado et al. 2006a). For methane, it was assumed that the parameter q_{max} is equal to the one of carbon dioxide, so that the parameter b was deduced from the value of $q_{max}b$ (Table 3). The comparison is shown in Fig. 8, where it can be observed that the model predicts the experimental curves adequately for most of the experiments. In order to evaluate the deviation from ideality in the adsorbed phase in this system, interaction factors (f_i) were introduced in (1), and their values were estimated by nonlinear regression:

$$q_i = \frac{Py_i\varepsilon_p}{RT\rho_p} + \frac{q_{\max,i}\, f_i b_i P y_i}{1 + \sum_{j=1}^{j=n} f_i b_j P y_j} \tag{7}$$

resulting in $f_{CO2} = 0.96$ and $f_{CH4} = 0.64$. These values would indicate that the carbon dioxide/methane selectivity of the resin (q_{CO2}/q_{CH4}) is higher than the ideal one deduced from the single component isotherms. However, it was observed that the improvement in the fitting quality considering these factors was quite small, suggesting that the ideal selectivity is more realistic for this system.

4.5 Carbon dioxide/methane separation by PSA using Amberlite IRA-900

The applicability of Amberlite IRA-900 to the separation of carbon dioxide/methane mixtures was studied in an experimental PSA setup using a single bed (Fig. 2). The cycle consisted of three consecutive steps: (i) pressurization with feed, (ii) feed at high pressure, and (iii) countercurrent blowdown. A scheme of the cycle is shown in Fig. 9.

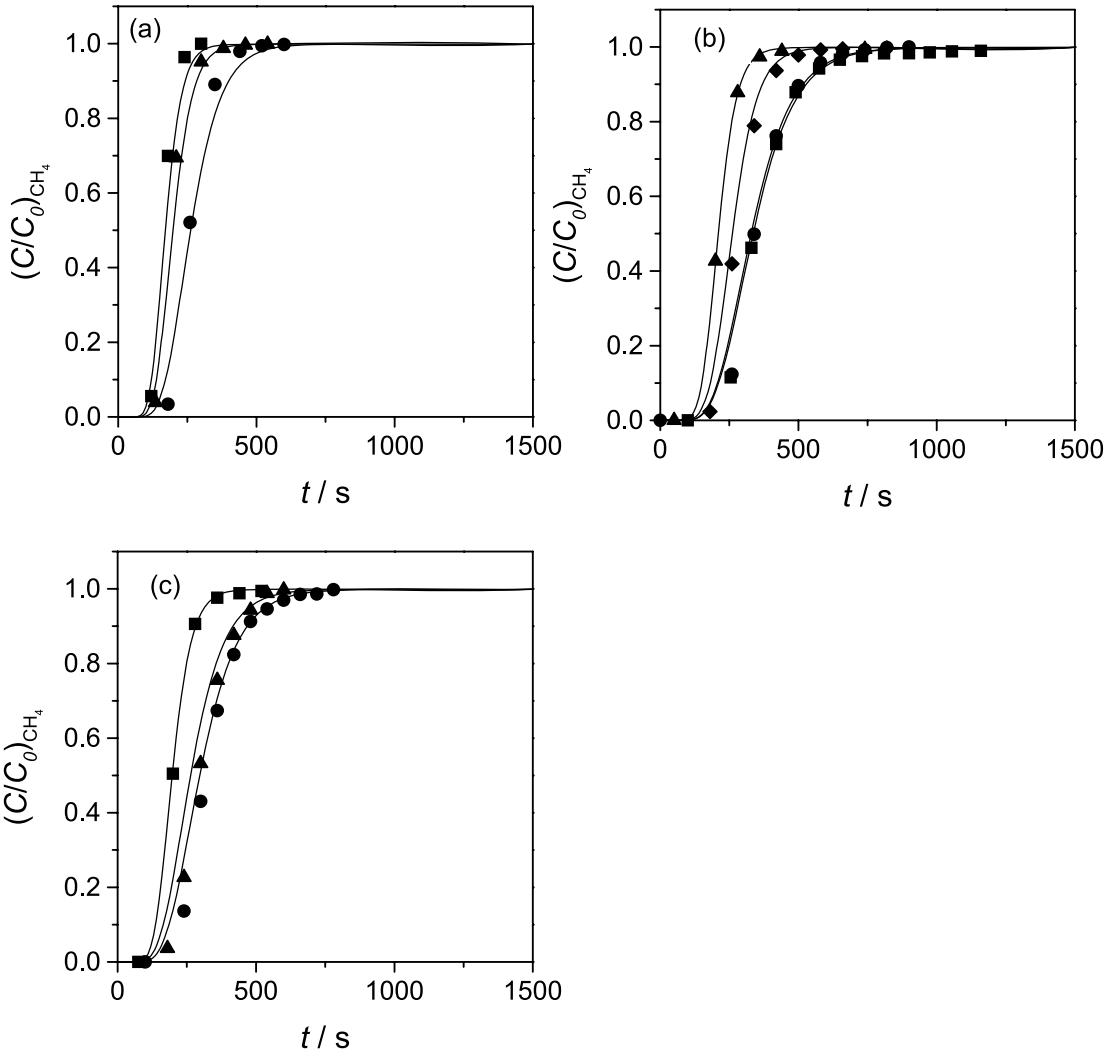

Fig. 7 Breakthrough curves of CH_4-He mixtures in silicalite. Experimental conditions in Table 2. *Continuous lines* are obtained with the model. (**a**) *Squares*, Run 11; *circles*, Run 12; *triangles*, Run 13. (**b**) *Squares*, Run 14; *circles*, Run 15; *triangles*, Run 16; *diamonds*, Run 17. (**c**) *Squares*, Run 18; *circles*, Run 19; *triangles*, Run 20

In this study, neither the effect of trace contaminants accompanying methane in landfill gas (sulphur-containing, aromatic, and chlorinated compounds), nor the effect of moisture, have been considered. These compounds should be removed prior to the proposed process if they were detrimental to the adsorption capacity of the basic resin. The performance of the PSA was analyzed for two feed compositions, 35 and 56% of carbon dioxide. The bed dimensions and the operating conditions are given in Table 5.

These conditions were selected within the range allowed in the experimental setup, in order to get the maximum methane purity in the product, and the maximum productivity. The validity of the model to simulate the PSA dynamics was checked by comparing the experimental values of product and extract compositions, methane recovery, and the productivity, with the ones predicted with the model (Table 5). The model parameters and equations for simulating the PSA performance are the same as those used in the previous section, except for the boundary conditions for the pressurization and blowdown steps, which were described elsewhere (Delgado et al. 2006a). The boundary conditions were proposed following the work of Da Silva and Rodrigues (2001). The results presented were obtained when the cycle reached the steady state, that is to say, the extract and product composition did not change in successive cycles. The similarity between the experimental and predicted results indicate that the model is valid for designing PSA systems based on the studied adsorbent. It was also observed that the estimated performance parameters were sensitive to the value of the LDF parameter (k_s) for carbon dioxide. As this parameter was estimated assuming that the internal mass transfer was macropore controlled (the diffusion time in (6) is calculated using the free molecular diffusivity for carbon dioxide-methane mixtures), it is confirmed that this

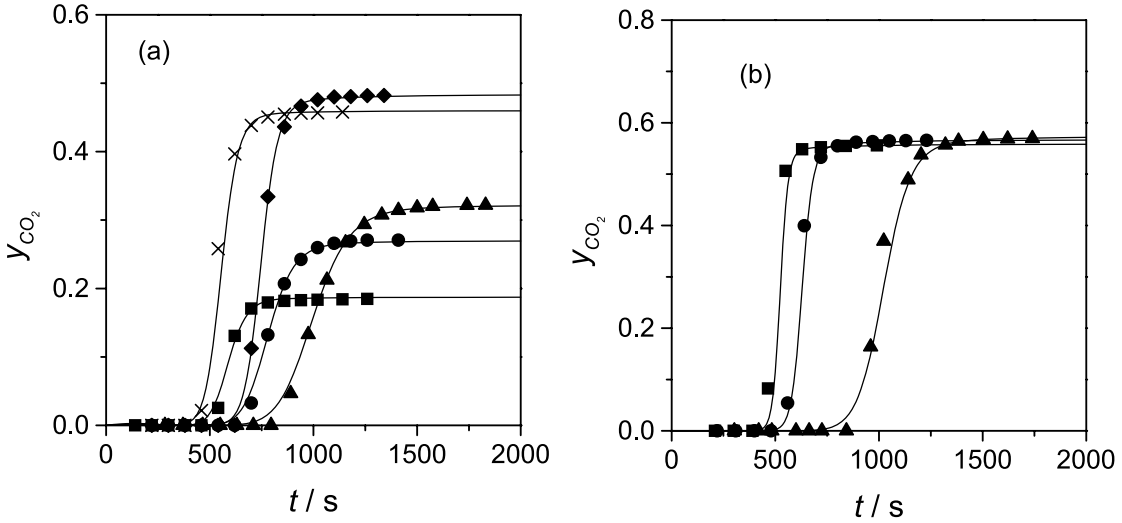

Fig. 8 Breakthrough curves of CO_2-CH_4 mixtures in silicalite. Experimental conditions in Table 4. *Continuous lines* are obtained with the model. (**a**) *Squares*, Run 21; *circles*, Run 22; *triangles*, Run 23; *diamonds*, Run 24; *crosses*, Run 25. (**b**) *Squares*, Run 26; *circles*, Run 27; *triangles*, Run 28

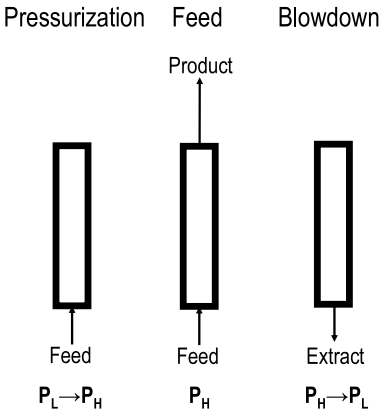

Fig. 9 Scheme of the studied PSA cycle. P_L and P_H are low and high pressures

assumption is valid for this system. It is observed that 97% methane can be obtained from a feed containing a 35% of carbon dioxide using Amberlite IRA-900, whereas this purity could not be reached from a feed with a 56% of carbon dioxide. According to model simulations, it would be necessary to increase the bed length by a factor of 2.3, or to reduce the low pressure in the cycle down to $4{\cdot}10^2$ Pa, and the feed flow rate down to $1.5{\cdot}10^{-7}$ m^3 s^{-1}, to obtain 97% methane in this case. The energy consumption of the proposed cycle has been estimated as 1.9 kWh per kg of methane product, assuming polytropic compression in the blowdown step (polytropic exponent = 1.4, compressor efficiency = 0.8). The productivity values obtained are lower than the value reported in the literature for carbon molecular sieves (0.045 kg_{CH4} kg_{resin} h^{-1}, Kapoor and Yang 1989). However, it must be noted that the productivity obtained with the basic resin could be higher than this value by reducing the cycle time. As the diffusion constant for carbon dioxide in the basic resin ($D/r_p^2 \approx 1$ s^{-1}, estimated as $k_s/15$, (6)) is much higher than the one obtained for carbon molecular sieves ($9{\cdot}10^{-4}$ s^{-1}, Kapoor and Yang 1989), the reduction of the cycle time does not affect the cycle performance for the basic resin negatively (which has been confirmed by simulation). For the carbon molecular sieve, the effect of this reduction could have a negative impact on the performance, because the mass transfer resistance in the adsorbent is much higher.

5 Conclusions

The adsorption of carbon dioxide and methane on Amberlite IRA-900 in OH-form packed in a fixed bed has been studied. The following conclusions can be withdrawn from this work:

(a) The carbon dioxide adsorption capacity of the bed initially decreased with the number of adsorption-desorption cycles, reaching a constant value thereafter. This capacity can be recovered by treating the resin with NaOH.
(b) The adsorption equilibrium parameters for both adsorbates have been obtained in the fixed-bed setup (Table 3), once the adsorption capacity of carbon dioxide got stable with the number of adsorption-desorption cycles. The value of the adsorption enthalpy for carbon dioxide (19 kJ mol^{-1}) suggests that this gas is physisorbed on the basic resin. This value was very similar to the one obtained in a volumetric installation.
(c) A model based on the LDF approximation was able to reproduce the breakthrough curves obtained with carbon dioxide-helium and methane-helium mixtures. This

Table 5 Parameters used in the simulations of the PSA system, operating conditions, and comparison between the experimental and the predicted performance of the studied PSA cycle

Parameter			
Particle radius, m			$2.8{\cdot}10^{-4}$
Particle density, kg m^{-3}			855
Particle tortuosity			4
Particle porosity			0.292
Particle heat capacity, J kg^{-1} K^{-1}			920
Bed length, m			0.125
Bed weight, kg			0.0126
Bed voidage fraction			0.42
Bed internal diameter, m			0.016
Column wall thickness, m			$2{\cdot}10^{-3}$
Wall heat capacity, J kg^{-1} K^{-1}			500
Wall density, kg m^{-3}			8000
Overall heat transfer coefficient, W m^{-2} K^{-1}			30

Operating conditions		Run 1	Run 2
y_F		0.35	0.56
Q_F, m^3 s^{-1}		$7.8{\cdot}10^{-7}$	$1.0{\cdot}10^{-6}$
P_H, Pa		$1.1{\cdot}10^{5}$	$1.1{\cdot}10^{5}$
P_L, Pa		$1.0{\cdot}10^{3}$	$1.5{\cdot}10^{3}$
t_{pres}, s		95	108
t_{feed}, s		30	15
t_{blow}, s		10	10
%CH_4 in product, %	Exp.	97	93
	Pred.	96	92
%CO_2 in extract, %	Exp.	48	66
	Pred.	43	62
% Methane recovery	Exp.	36	26
	Pred.	32	22
Productivity, kg_{CH4} kg_{resin} h^{-1}	Exp.	0.029	0.018
	Pred.	0.024	0.012

model was also valid for simulating the breakthrough curves obtained with carbon dioxide-methane mixtures, using the extended Langmuir model as the multicomponent adsorption equilibrium isotherm.

(d) The applicability of Amberlite IRA-900 to the separation of carbon dioxide/methane mixtures was studied in an experimental PSA setup using a single bed. The model employed to simulate the breakthrough curves was also adequate to simulate the PSA performance, introducing the appropriate boundary conditions for the pressurization and blowdown steps. A product with a 97% of methane was obtained experimentally from a feed containing a 35% of carbon dioxide. For a feed with a 56% of carbon dioxide, this was not possible. According to model simulations, 97% methane could be obtained with the same PSA configuration increasing the bed length, or reducing the low pressure in the cycle and reducing the feed flowrate.

Acknowledgement Financial support from the "Ministerio de Educación y Ciencia" of Spain through project CTQ2004-00320/PPQ is gratefully acknowledged.

References

Cavenati, S., Grande, C.A., Rodrigues, A.E.: Upgrade of methane from landfill gas by pressure swing adsorption. Energy Fuels **19**, 2545–2555 (2005)

Da Silva, F., Rodrigues, A.E.: Propylene/propane separation by vacuum swing adsorption using 13X zeolite. AIChE J. **47**, 341–357 (2001)

Delgado, J.A., Uguina, M.A., Sotelo, J.L., Ruiz, B., Gómez, J.M.: Fixed-bed adsorption of carbon dioxide/methane mixtures on silicalite pellets. Adsorption **12**, 5–18 (2006a)

Delgado, J.A., Uguina, M.A., Gomez, J.M., Ortega, L.: Adsorption equilibrium of carbon dioxide, methane and nitrogen onto Na- and H-mordenite at high pressures. Sep. Purif. Technol. **48**, 223–228 (2006b)

Do, D.D.: Adsorption Analysis: Equilibria and Kinetics, p. 61. Imperial College Press, Singapore (1998)

Engelhard Corporation: Adsorption processes for natural gas treatment, a technology update, www.engelhard.com (2005)

Farooq, S., Ruthven, D.M.: Heat effects in adsorption column dynamics. 1. Comparison of one- and two-dimensional models. Ind. Eng. Chem. Res. **29**, 1076–1084 (1990)

Gomes, V.G., Hassan, M.M.: Coalseam methane recovery by vacuum swing adsorption. Sep. Purif. Technol. **24**, 189–196 (2001)

Kapoor, A., Yang, R.T.: Kinetic separation of methane-carbon dioxide mixture by adsorption on molecular sieve carbon. Chem. Eng. Sci. **44**, 1723–1733 (1989)

Khoo, H.H., Tan, R.B.H.: Life cycle investigation of CO_2 recovery and sequestration. Environ. Sci. Technol. **40**, 4016–4024 (2006)

Levenspiel, O.: Chemical Reactor Engineering, 3rd edn., p. 311. Wiley, New York (1999)

Li, S., Martinek, J.G., Falconer, J.L., Noble, R.D., Gardner, T.Q.: High-pressure CO_2/CH_4 separation using SAPO-34 membranes. Ind. Chem. Eng. Res. **44**, 3220–3228 (2005)

Madsen, N.K., Sincovec, R.F.: PDECOL, general collocation software for partial differential equations [D3]. ACM Trans. Math. Softw. **5**, 326–351 (1979)

Pilarczyk, E., Knoblauch, K.: In: Li, N., Strathmann, H. (eds.) Separation Technology, p. 522. Eng. Foundation, New York (1988)

Ruthven, D.M., Farooq, S., Knaebel, K.S.: Pressure Swing Adsorption. VCH, New York (1994), Chapter 2 and pp. 208, 244

Schroter, H.J., Juntgen, H.: In: Rodrigues, A.E., LeVan, M.D. (eds.) Adsorption: Science and Technology, NATO ASI, vol. 158, pp. 269. Kluwer, Dordrecht (1989)

Sircar, S. Kumar, R.: Adiabatic adsorption of bulk binary mixtures: analysis by constant pattern model. Ind. Eng. Chem. Process. Des. Dev. **22**, 271–80 (1983)

Valenzuela, D.P., Myers, A.L.: Adsorption Equilibrium Data Handbook, pp. 47–49. Prentice Hall, Englewood Cliffs (1989)

Wakao, N., Kaguei, S., Nagai, H.: Effective diffusion coefficients for fluid species reacting with first order kinetics in packed bed reactors and discussion on evaluation of catalyst effectiveness factors. Chem. Eng. Sci. **33**, 183–187 (1978)

Yang, R.T.: Gas Separation by Adsorption Processes. Imperial College Press, Singapore (1997), pp. 4, 124

Yang, R.T.: Adsorbents: Fundamentals and Applications, p. 273. Wiley, New Jersey (2003)

Yong, Z., Rodrigues, A.E.: Hydrotalcite-like compounds as adsorbents for carbon dioxide. Energy Convers. Manag. **43**, 1865–1876 (2002)